THE JOURNAL OF PHYSICAL CHEMISTRY A

Article

pubs.acs.org/JPCA

Solvated States of Poly-L-alanine α-Helix Explored by Raman Optical Activity

Shigeki Yamamoto,*[,†] Tatsuya Furukawa,[‡] Petr Bouř,*[,§] and Yukihiro Ozaki[‡]

[†]Department of Chemistry, Graduate School of Science, Osaka University, Toyonaka, Osaka 560-0043, Japan

[‡]Department of Chemistry, School of Science and Technology, Kwansei Gakuin University, Gakuen 2-1, Sanda, Hyogo 669-1337, Japan

[§]Institute of Organic Chemistry and Biochemistry, Academy of Sciences, 166 10 Prague, Czech Republic

Supporting Information

ABSTRACT: Raman optical activity (ROA) reveals surprising details of the secondary structure of polypeptides and proteins in solution phase. Yet specific spectral features, such as in the extended amide III region of hydrated α-helix, did not seem explicable by the generally accepted sensitivity of ROA to the local conformation. This is reconciled in the present study by simulations of ROA spectra for model α-helical structures. Two positive ROA peaks often observed at around 1340 and 1300 cm^{-1} for polypeptides and proteins have been assigned to two types of solvated α-helices; one is stable in hydrophilic environment where amide groups make hydrogen bonds to solvent molecules or polar side chains (~1340 cm^{-1}), and the other is supported by a hydrophobic environment without the possibility of external hydrogen bonds (~1300 cm^{-1}). For poly-L-alanine (PLA), regarded as a good model of α-helical structure, the experimentally observed relative intensity ratio of the two ROA bands has been explained by a conformational equilibrium depending on the solvent polarity. The intensities of the bands reflect solvated and unsolvated α-helical geometries, with peptide backbone torsional angles (ϕ_{i+1}, ψ_i) of (−66°, −41°) and (−59°, −44°), respectively. Quantum-mechanical simulations of the ROA spectra utilizing the normal mode optimization and Cartesian tensor transfer methods indicate, however, that the change in dielectric constant of the solvent is the main factor for the spectral intensity change, whereas the influence of the conformational change is minor.

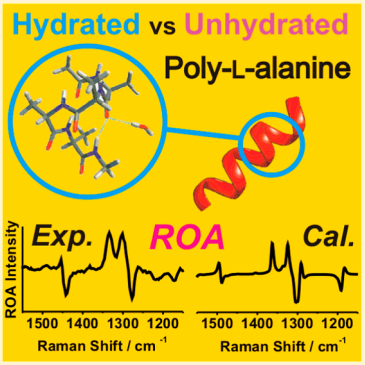

INTRODUCTION

Solvation of peptides and proteins has been attracting attention for a long time,[1−4] but the influence of solvent molecules on peptide structure remains rather unexplored. For example, the proton NMR spectroscopy frequently used to study protein hydration[5] has serious limitations for solutions due to its relatively slow time response. Fast exchange of the solvated molecules in the hydration sphere with the bulk solvent molecules can hamper specific NMR signal. FTIR bands of polypeptides and proteins in deuterated water would be sensitive to the solvation of α-helices, but the assignments and explication are still in debates.[6−9]

The interplay between protein secondary structure and the environment has been analyzed by high-resolution X-ray crystallography.[10−14] Water-induced distortion of α-helices in three refined X-ray structures of proteins was detected by Blundell et al.[10] The conformational difference between residues in hydrophilic and hydrophobic environments can be best recognized in a probability plot of peptide backbone torsional angles of neighboring residues, ϕ_{i+1} and ψ_i, which reflect the tilting of hydrogen-bonded C═O from the line connecting C_i and N_{i+4}. For the residues bonded to a water molecule or peptide side chain, average values of (ϕ_{i+1}, ψ_i) are (−66°, −41°) and referred to as α_o, for residues without such hydrogen bonds the values are (−59°, −44°) and referred to as α_c (Figure 1).

A more detailed analysis of hydrated α-helices in 35 high-resolution X-ray crystal structures[11] revealed three types of hydrogen bonding between peptide backbone and water

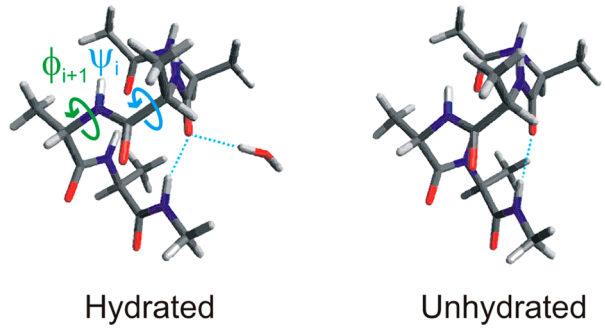

Figure 1. Hydrated (left) and unhydrated (right) $(Ala)_4$ fragments, with the peptide torsional angles (ϕ_{i+1}, ψ_i) of (−66°, −41°) and (−59°, −44°), respectively.

Received: January 23, 2014
Revised: March 24, 2014
Published: April 23, 2014

molecules: *external* hydration, *three-centered* hydration, and *water-inserted* hydration. The external type is the most common,[13,15] where a water molecule is externally bonded only to the $(C{=}O)_i$ group which is already hydrogen-bonded to the $(NH)_{i+4}$ group (Figure 1). Because the difference in the torsional angles between α_o and α_c is very small, it is difficult to distinguish it by conventional techniques. Therefore, the chiral spectroscopy of vibrational Raman optical activity (ROA)[16−19] has been suggested for this purpose.[15]

ROA is measured as a small differences in Raman scattering intensities corresponding to right- and left-circularly polarized light.[16−21] It is particularly useful for studying solution structures of biomolecules.[22−25] Extensive studies have been done on proteins, often relying on comparisons of the spectra in solution with protein crystal structures.[22,26,27] ROA bands in the extended amide III region[22] including deformations of CH and NH groups observed between 1400 and 1300 cm^{-1} are particularly sensitive to the secondary structure of proteins.[27−33] In the case of α-helical peptides and proteins, two positive ROA bands in this region have been assigned to two types of solvated α-helices. A band at ∼1340 cm^{-1} is typical for a hydrophilic environment, whereas the other at ∼1300 cm^{-1} is for a hydrophobic one.[15,28,29] Amide I and other ROA bands are also sensitive to the secondary structure; however, they are less susceptible to the differences associated with the two types of α-helices.

Because of the high sensitivity to the structure, these hydrated and unhydrated ROA bands of the extended amide III regions were suggested to correspond to the more open α_0 and the canonical α_c conformations, which was supported by experimental ROA analyses of peptides and proteins.[15] For example, for peptides containing highly hydrated α-helices, such as human serum albumin and α-helical poly-L-lysine, the hydrated ROA band at ∼1340 cm^{-1} is dominant and the band at ∼1300 cm^{-1} is weak. On the other hand, more amphiphilic proteins such as insulin shows only weak hydrated ROA band or sometimes just as a shoulder.[22] Moreover, the conformational change of the hydrated α-helix was observed as a vanishing of the ROA peak at ∼1340 cm^{-1} during denaturation of some α-helical proteins. A similar effect can be observed during the α-helix-to-β-sheet conversion of poly-L-lysine in aqueous solution by increasing temperature.[27] The α-helical structure in human lysozyme changes to the polyproline II (PP-II) helical structure in an amyloidogenic prefibrillar intermediate state.[28] When the amyloidogenic intermediate of bovine insulin converts to the native state, the hydrated α-helical peak is recovered.[34] The conversion was also observed for the molten globule (A-state) of native bovine α-lactalbumin.[29] These observations suggest that the conversion via the hydrated α-helices is a standard process in protein folding. However, factors underlying the changes in α-helical ROA bands have not been elucidated completely so far.

Poly-L-alanine (PLA) is the simplest chiral peptide model, secondary structure of which has been studied extensively by spectroscopic methods.[35−38] The peptide is known to adopt the α-helical conformation in strongly polar organic solvents,[37−40] such as dichloroacetic acid (DCA),[40] which is a suitable model system for α-helices in proteins. A ROA spectrum of PLA in DCA contains the hydrated and unhydrated positive peaks at 1338 and 1304 cm^{-1}; the hydrated band is slightly stronger.[15] In a more hydrophobic mixed solvent of $CHCl_3$/DCA = 7/3 (v/v), the relative intensity of the hydrated ROA band diminishes. The intensity ratio of the positive 1338 and 1304 cm^{-1} ROA bands was suggested as a marker for the ratio of α_c and α_o conformations.[15] However, this suggestion ignores possible influence of the differences in the dielectric constant of the surrounding solvent. As shown below, this is consistently reconciled by the present simulations. In fact, the dielectric constant (ε_r) of the surrounding solvent is a dominant factor for the whole phenomenon.

Owing to recent developments of theory, computational techniques, and hardware, quantum mechanical calculations of ROA spectra became a routine tool for interpretations of experimental results.[41] The simulations succeeded in reproduction of ROA spectra for small molecules,[42−49] peptides,[50−52] even proteins.[53,54] In spite of previous effort, however, the experimental ROA spectral pattern of PLA in the extended amide III region could not be reproduced so far.[55−57] The two positive peaks at ∼1340 and ∼1300 cm^{-1}, and also a negative peak at ∼1280 cm^{-1}, have not been satisfactorily reproduced even in simulations considering the solvent explicitly.[57] Typically, the positive peak at ∼1340 cm^{-1} has been calculated as too weak or even as a negative peak.[55−57] Available experiments suggest that difficulties in modeling are caused by the exceptional sensitivity of the extended amide III ROA bands to the solvation states.

Some inconsistencies in the simulations may have been caused by inadequate model geometries. As mentioned in ref 55, standard optimization of $(Ala)_{10}$ changes the peptide backbone structure from α-helix to 3_{10}-helix at the peptide termini. This is not dependent on the length,[57] and would cause small changes in the ϕ and ψ angles. Therefore, in our study, a partial optimization is carried out in the normal mode coordinates[58,59] to achieve a more controlled backbone structure. Note that normal modes of lower frequencies (typically below 300 cm^{-1}) can be fixed in the normal mode optimization (NMO), while the higher frequency modes of spectroscopic interest are fully relaxed. The NMO enables us to test the two sets of torsional angles, for the hydrated and unhydrated α-helices, together with the effect of the solvent.

In this paper the solvent was modeled by using the conductor-like continuum solvent model (CPCM).[60,61] Although the model does not completely describe hydrogen bonds in polar solvents,[42,48,62] it can provide the main trends caused by the solvation.[50−53] Also an explicit solvent model was tested in order to estimate the error caused by the CPCM approximation.

Main factors affecting the extended amide IIII ROA bands are explored in this paper. We thus hope to contribute to elucidation of protein folding processes, particular to those including conversions of hydrated α-helices.

METHODS

Initial structures of Ac-$(Ala)_{18}$-NHMe were created by the Avogadro software[63] with peptide torsional angles (ϕ, ψ) set to (−66°, −41°) for the hydrated α-helix and to (−59°, −44°) for the unhydrated one. The peptides were terminally capped by methyl groups to avoid possible interactions with the solvent via the terminal amide groups. All models in this study are terminally capped. ROA and Raman spectra were calculated using the Cartesian coordinate tensors transfer (CCT)[64,65] method, i.e. force field and derivatives of the ROA and Raman tensors were calculated quantum-mechanically (QM) for smaller model fragments with the hydrated or the unhydrated structure, and then transferred to the original $(Ala)_{18}$ peptide. The Gaussian program is used for the QM computations.[66]

dx.doi.org/10.1021/jp500794s | J. Phys. Chem. A 2014, 118, 3655−3662

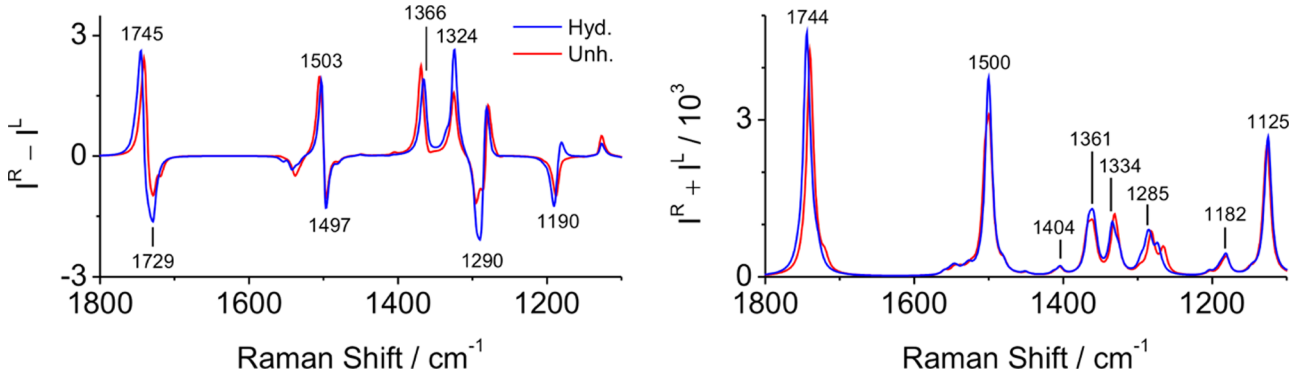

Figure 2. Comparison of ROA (left) and Raman (right) spectra of PLA calculated in vacuum for the hydrated (blue line, frequencies indicated) and the unhydrated (red line) α-helical structure at the B3LYP/6-311++G** level.

Typically, the B3LYP[67]/6-311++G** level was used, but other functionals, basis sets, and various solvent models (CPCM) were also tested as specified below.

An $(Ala)_6$ fragment (i.e., Ac-$(Ala)_6$-NHMe) created from the original $(Ala)_{18}$ molecule by using the MCM program[68] was also terminated by methyl groups. For control computations, a smaller $(Ala)_4$ fragment was adopted as well. Fragment geometries were optimized by NMO with fixed normal modes below 300 cm^{-1}, and the property tensors were calculated. The tensors were transferred to $(Ala)_{18}$, atom by atom, considering the origin-dependence of the tensors. As seen in Figure S1 (Supporting Information), all monomer units of each fragment were overlapped with the other fragments in the appropriate parts of the target molecule. The tensors from different fragments were averaged for each atom pair with weights dependent on the distance between the fragment and the center of atom pair.[64] Finally, the backscattering Raman and ROA spectra were generated using Lorentzian functions of full-width at half-maximum of 10 cm^{-1} and Boltzmann temperature correction of the intensities at 300 K.

The CCT method enabled us to test multiple solvent models and to use a large basis set (6-311++G**) which is required for proper modeling of the spectra. It is known that this approximation sometimes exhibits a limited precision for α-helices.[65,69] The CCT result for $(Ala)_{18}$ performed with 6-31G** basis set was compared to a full DFT calculation (Figure S2, Supporting Information). We can see the CCT method does provide frequencies shifted if compared to the reference, nevertheless the principal spectral pattern is conserved as also discussed in ref 65.

For the alternative model of the solvent, one DCA molecule was attached to the $(Ala)_5$ fragment in the hydrated α-helical structure, then the geometry was optimized using the CPCM(dichloroethene) solvent with the fixed ϕ and ψ angles. The optimized bonding pattern of the DCA was copied to the $(Ala)_{18}$ with 18 DCA molecules. The NMO and the tensors calculations were done with the attached DCA molecule in vacuo, then transferred to the $(Ala)_{18}$ peptide with 18 DCA molecules.

RESULTS AND DISCUSSION

Figure 2 shows the calculated ROA and Raman spectra of the $(Ala)_{18}$ based on the hydrated and unhydrated α-helical structures at the B3LYP/6-311++G** level of theory. The Raman spectra are very similar to the reported experimental spectra of α-helical PLA,[70] and also to our measured spectrum displayed in Figure S3 (Supporting Information). For both forms, the main features of ROA spectra also well agree with the experimental results obtained by McColl et al. shown in Figure 3.[15] The experimental positive/negative ROA couplet of

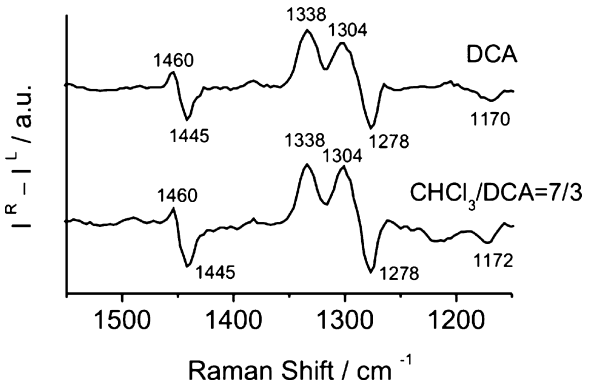

Figure 3. Experimental ROA spectra of PLA reproduced from ref 15 measured for PLA solutions (75 mg/mL) in DCA and a mixed solvent of $CHCl_3$/DCA = 7/3 (v/v). The weak negative peak at around 1220 cm^{-1} in the mixed solvent is an artifact from the instrument.

the amide I band at 1650 cm^{-1} and the methyl deformation bands at 1450 cm^{-1} are calculated at 1740 and 1500 cm^{-1} for both structures, with stronger relative intensities than in the experiment. The +/+/− experimental ROA peaks at 1338, 1304, and 1278 cm^{-1} are simulated at 1366, 1324, and 1290 cm^{-1}, where a noticeable difference between the hydrated and unhydrated structures is apparent in calculated intensities.

In accord with previous assignments,[55−57] the positive peaks calculated at 1366 and 1324 cm^{-1} come from C^α-H bending vibrations, where the hydrogen atoms bend approximately along the C^α−N and C^α−C(=O) bonds, respectively (Figure S4). Following previous literature, we refer to them as types I and II, respectively. The calculated negative ROA peak at 1290 cm^{-1} originates from the amide III band, a combination of δ (NH) in the amide plane and δ (C^α-H) with hydrogens bent along the C^α−C^β bonds. In the calculation for the hydrated structure, the intensity of the type I band is weaker than the type II band. However, for the unhydrated structure, the band I is stronger than II. The exceptional sensitivity of these bands to the conformation is evident in Figure 2.

Note that in the experiment,[15] the intensity ratio of the bands (I_I/I_{II}) is 1.26 in DCA and 1.05 in a mixed solvent of $CHCl_3$/DCA = 7/3 (v/v). The calculated ratios are 0.72 and 1.43 for the hydrated and unhydrated structures, respectively. In other

dx.doi.org/10.1021/jp500794s | J. Phys. Chem. A 2014, 118, 3655−3662

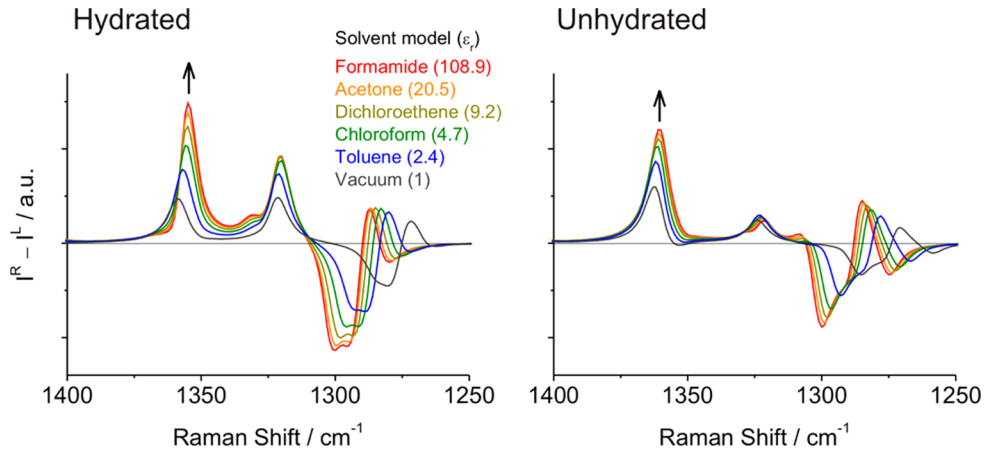

Figure 4. Effect of the dielectric constant used in the CPCM solvent model with B3LYP/6-311++G** method on calculated ROA spectra of PLA in the hydrated (left) and unhydrated (right) α-helical conformations. Solvent model and relative dielectric constants are indicated.

words, the calculated trend is opposite to the conventional explanation of the experiment, i.e., equilibrium between the hydrated and unhydrated structures depending on solvent polarity. This and further calculations suggest that the structural difference is not the main factor determining the intensity ratio, but dielectric constant of the surrounding solvent is important as well.

Variations of the calculated ROA intensities in the extended amide III region for various dielectric constant (ε_r) are displayed in Figure 4. $(Ala)_4$ fragment adopted as a source of the tensors in this CCT calculation results in a quite similar spectra as for the longer $(Ala)_6$. For the hydrated α-helical structure of PLA, the calculated band I at 1360 cm^{-1} increases its intensity and shifts to lower frequency with increasing ε_r, but the band II at 1320 cm^{-1} is nearly constant under the CPCM models. I_I/I_{II} is about 1.5 times larger for formamide as a solvent (ε_r = 108.9), if compared to vacuum. The calculated amide III peak becomes stronger and shifted to higher frequencies. The ROA spectral pattern of the extended amide III region is sensitive to the dielectric constant of the surrounding medium. For the unhydrated structure, I_I/I_{II} becomes about 5. The intensity ratios for the two structures are plotted against ε_r in Figure 5, together with the experimental ratios based on ref 15. While the calculated ratios for the unhydrated structure are always over 4 times larger than in experiment, the ratios for the hydrated structure are very close to the experimental values. The calculations with $(Ala)_6$ provide similar ratio, and the agreement with the experiment is clearly better for the hydrated structure. The ratio for the unhydrated ones becomes nearly 2 with the CPCM model of dichloroethene, i.e. is far from the experiment. Similar tendencies are observed in the calculations with the smaller 6-31+G** basis set, while the ratios were larger in all cases as found in Figure S5 (Supporting Information). These results indicate that the unhydrated α-helical structure is a minor conformation under given experimental conditions.

Therefore, the experimentally observed ratios can be explained by a variation of the dielectric constant around the hydrated α-helical structure, not by the geometry change. According to the B3LYP/6-311++G** calculations with the $(Ala)_6$ fragments with the different geometries, the ratio should decrease from 1.77 to 1.22 for given increase of ε_r, not increase from 1.05 to 1.26 as in the experiment. Therefore, the changes in the dielectric constant govern the experimental ROA. This

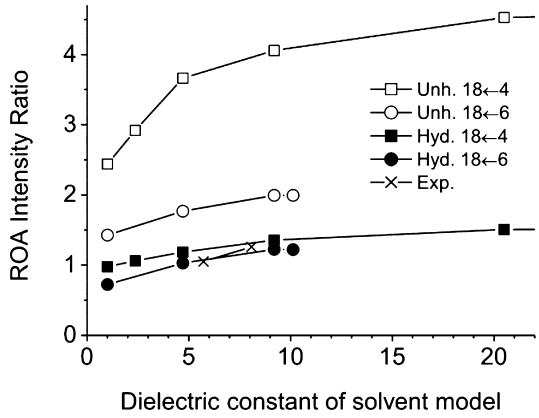

Figure 5. Dependence of the intensity ratio (I_I/I_{II}) of the two ROA bands of PLA (at ~1360 cm^{-1}, I_I, and at ~1330 cm^{-1}, I_{II}) on the dielectric constant for the hydrated (filled symbols) and unhydrated (empty symbols) structures calculated at the B3LYP/6-311++G** level based on the $(Ala)_6$ (circle) and $(Ala)_4$ (square) fragments in the CCT scheme. The experimental ratios (×) are based on ref 15. The ε_r of the mixed solvent ($CHCl_3$/DCA=7/3, v/v) in the experiment was estimated as 5.7 by a weighted-average ($CHCl_3$, ε_r = 4.7, and DCA, ε_r = 8.1).

suggests that PLA adopts the hydrated geometry in both solvents. In fact, PLA can be solvated by DCA even in the mixed $CHCl_3$/DCA solvent. This is consistent with a low-solubility of PLA in pure $CHCl_3$ (less than 0.1 mg/mL at room temperature). The DCA concentration in the mixed solvent is 3.6 M, which corresponds to three DCA molecules per alanine residue for the experimental concentration of PLA of 75 mg/mL. However, PLA in the mixed solvent will still feel the dielectric constant of the bulk $CHCl_3$.

The ROA spectra of PLA calculated under these assumptions for the hydrated structure (Figure 6) compare well to the experimental results in Figure 3. CPCM models of dichloroethene (ε_r = 9.2) and $CHCl_3$ (4.7) are selected to best mimic the experimental solvents of DCA (8.1) and $CHCl_3$/DCA = 7/3 (5.7, a weighted average). The small experimental changes in the extended amide III region are well-reproduced by the calculations. A good agreement exhibits also the relative intensity of the δ (CH_3) ROA couplet at 1490 cm^{-1}, close to the experimental wavenumber of 1460 cm^{-1}. Most probably, PLA thus adopts the hydrated conformation only.

dx.doi.org/10.1021/jp500794s | J. Phys. Chem. A 2014, 118, 3655−3662

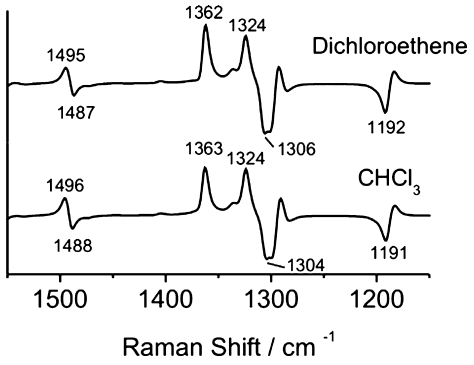

Figure 6. Simulated ROA spectra of PLA in the hydrated α-helical structure. Calculation level: B3LYP/6-311++G**/CPCM.

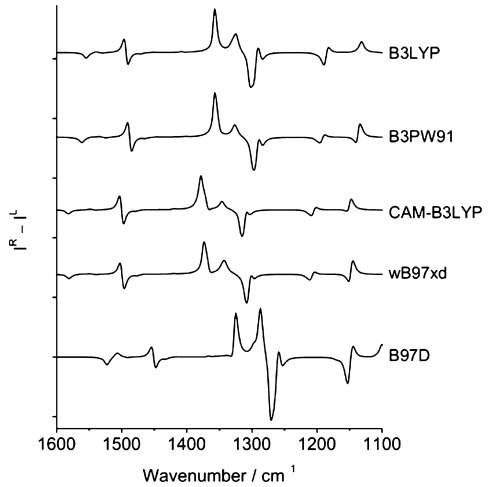

Figure 7. Calculated ROA spectra of PLA in the hydrated α-helical structure as obtained with the 6-31+G**/CPCM(dichloroethene) model and the B3LYP, B3PW91, CAM-B3LYP, wB97xd, and B97D functionals.

While the fwhm of 10 cm^{-1} used in the Lorentzian fit for the calculations is the same as the spectral resolution in the experiment, the band I and II are somewhat broader in the experiment. This inhomogeneous broadening may reflect the flexibility of PLA as seen for small molecules previously, where more flexible dipeptides provide ROA spectra with broader and fewer characteristic features.[71] It is true that explicit solvent molecules can also participate on the spectral shape, however, extensive averaging is required for such modeling which is not possible for PLA.[42,48] Fortunately, participation of explicit solvent molecules is most pronounced in the lowest-frequency region below about 400 cm^{-1},[72,73] far from the amide III region.

The origin of the solvent dependence of the type I and II amide III ROA bands are examined by separately considering the effect of the force field and the polarization on the ROA intensities in the cases of CPCM models of dichloroethene and $CHCl_3$. The combination of the force field calculated with the $CHCl_3$ model and the polarizabilities (the usual α, G' and A tensors) with the dichloroethene model results in I_I/I_{II} of 1.05. This is similar to that of the original $CHCl_3$ result of 1.03. However, the combination of the force field calculated with the dichloroethene and the polarizability obtained with the $CHCl_3$ gives the ratio of 1.25, which is close to the original dichloroethene result of 1.22. These results mean that the influence of ε_r on the force field is the main reason for the ratio change and that on the polarizability is minor. For all vibrational modes in the type I band, frequency differences between the $CHCl_3$ and the dichloroethene solvent models are smaller than 0.2 cm^{-1}. By considering typical experimental ROA spectral resolution of ~10 cm^{-1}, it is somewhat surprising that the ROA intensity ratio is influenced by such very small frequency difference. In some sense, ROA is amplifying the force field difference as resultant intensity change in the extended amide III region. Interestingly, only the band *I* ROA intensity changes with increasing ε_r ($CHCl_3$ → dichloroethene); the band II intensity remains nearly identical.

Possible computational error can be estimated in part from the functional dependence, and it does not seem to radically affect the main trends (Figure 7). The spectral patterns obtained with five different functionals are similar, perhaps except for the simplest B97D[74] GGA method. The I_I/I_{II} ratios obtained by the B3LYP, B3PW91,[75] CAM-B3LYP,[76] and wB97xd[77] functionals are quite similar. The frequencies are shifted to lower values for B3LYP and B3PW91 if compared to the newer CAM-B3LYP and the wB97xd methods. For all the functionals, the I_I/I_{II} ratio increases with ε_r.

Finally, the role of the explicit solvation is documented in Figure 8. In the optimized geometry, the C═O of amide group is bonded to both the DCA molecule and the amide NH group. The +/+/− extended amide III ROA peaks are calculated to be 1370, 1330, and 1298 cm^{-1}, quite similar to the CPCM results of 1357, 1324, and 1289 cm^{-1}. The I_I/I_{II} ratio obtained for the explicit model is 1.2, closer to the experimental value of 1.26 in DCA than that of 0.9 calculated without the DCA molecules (by erasing the intensity tensors of the DCA). Nevertheless, the precision of the implicit calculation seems to be sufficient to understand the phenomenon. The CPCM approach can additionally account for the solvent averaging, which is not easy in an explicit model.

ROA bands of proteins in the extended amide III region can be more influenced by the changes in the dielectric constant than by the structural changes of α-helices, as explored for PLA in this study. For the highly hydrated proteins, the α-helices will be more exposed to bulk water and feel a high dielectric constant, compared to more amphiphilic proteins where α-helices are less solvent-exposed and feel lower dielectric constant of neighboring peptide chains. For example, the hydrated ROA bands are stronger in bovine α-lactalbumin and equine lysozyme than in hen and human lysozymes.[15] This can be related to the differences in solvent-exposure as measured by NMR,[78] and not to the structural difference proposed previously.[15] The vanishing of the hydrated α-helical ROA band at ~1340 cm^{-1} in the denaturation processes of proteins[28,29,34] can be interpreted in terms of the solvent-exposure.

CONCLUSIONS

We simulated ROA spectra of a number of hydrated and unhydrated α-helical PLA structures to explain previously observed experimental features in peptides and proteins. The simulations were based on the density functional theory, significantly facilitated by the normal mode optimization and the tensor transfer techniques. Specific peptide conformations and dielectric constants of the solvent could be controlled in the simulations. For the first time, we could consistently reproduce the experimental ROA pattern in the extended amide III region of PLA. Unlike proposed previously, the

dx.doi.org/10.1021/jp500794s | J. Phys. Chem. A 2014, 118, 3655−3662

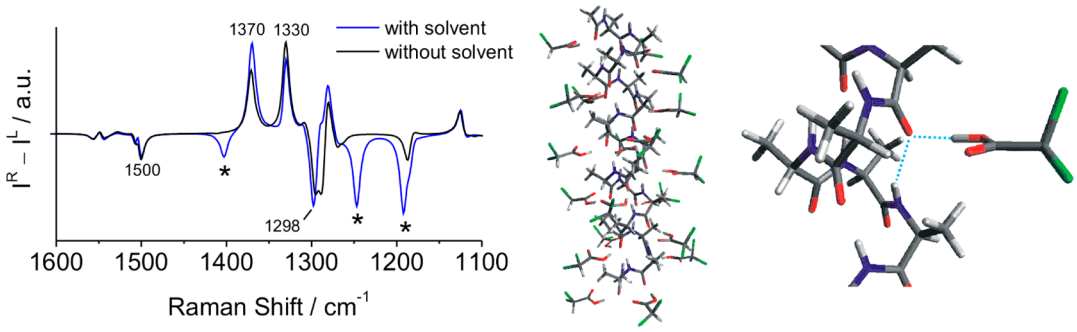

Figure 8. ROA spectra of $(Ala)_{18}$ as calculated with (blue line, model structure shown) and without (black line) 18 DCA molecules, at the B3LYP/6-31+G** level. The asterisks (*) indicate peaks of DCA molecules.

conformational equilibrium between the hydrated and unhydrated α-helices of PLA is not the main reason for the changes in intensity ratio of the two extended amide III marker bands. Instead, our results suggest that changes in the dielectric constant of the solvent are the predominant factor determining the ROA intensities. The ability of the ROA bands to distinguish solvent polarity in the vicinity of α-helix will be a useful tool for studies of protein folding often comprising conversion of hydrated α-helices.

■ ASSOCIATED CONTENT

Supporting Information

Scheme of the tensor transfer, calculated spectra, and atomic vibrations. This material is available free of charge via the Internet at http://pubs.acs.org/.

■ AUTHOR INFORMATION

Corresponding Authors

*(S.Y.) E-mail: aporoa@gmail.com. Telephone: +81-6-6850-5412.

*(P.B.) E-mail:bour@uochb.cas.cz. Telephone: +420-220-183-348.

Notes

The authors declare no competing financial interest.

■ ACKNOWLEDGMENTS

The work was supported by the JSPS fellowship (to S.Y.), and in part by the Academy of Sciences (M200550902) and Grant Agency (P208/11/0105) of the Czech Republic.

■ REFERENCES

(1) Schoenborn, B. P.; Garcia, A.; Knott, R. Hydration in Protein Crystallography. *Proc. Biophys. Mol. Biol.* **1995**, *64*, 105−119.

(2) Savage, H.; Wlodawer, A. Determination of Water Structure around Biomolecules Using X-Ray and Neutron Diffraction Methods. *Methods Enzymol.* **1986**, *127*, 162−183.

(3) Jeffrey, G. A.; Saenger, W. *Hydrogen Bonding in Biological Structures*; Springer-Verlag: Berlin, 1994.

(4) Gregory, R. B. *Protein-Solvent Interactions*; CRC Press: New York, 1995.

(5) Otting, G.; Liepinsh, E. Protein Hydration Viewed by High-Resolution Nmr Spectroscopy: Implications for Magnetic Resonance Image Contrast. *Acc. Chem. Res.* **1995**, *28*, 171−177.

(6) Brewer, S. H.; Tang, Y.; Vu, D. M.; Gnanakaran, S.; Raleigh, D. P.; Dyer, R. B. Temperature Dependence of Water Interactions with the Amide Carbonyls of A-Helices. *Biochemistry* **2012**, *51*, 5293−5299.

(7) Manas, E. S.; Getahun, Z.; Wright, W. W.; Degrado, W. F.; Vanderkooi, J. M. Infrared Spectra of Amide Goups in a-Helical Proteins: Evidence for Hydrogen Bonding between Helices and Water. *J. Am. Chem. Soc.* **2000**, *122*, 9883−9890.

(8) Haris, P. I.; Chapman, D. The Conformational Analysis of Peptides Using Fourier Transform Ir Spectroscopy. *Biopolymers* **1995**, *37*, 251−263.

(9) Reisdorf, W. C.; Krimm, S. Infrared Amide I′ Band of the Coiled Coil. *Biochemistry* **1996**, *35*, 1383−1386.

(10) Blundell, T.; Barlow, D.; Borkakoti, N.; Thornton, J. Solvent-Induced Distorsions and the Curvature of a-Helices. *Nature* **1983**, *306*, 281−283.

(11) Sundaralingam, M.; Sekharudu, Y. C. Water-Inserted a-Helical Segments Implicate Reverse Turns as Folding Intermediates. *Science* **1989**, *244*, 1333−1337.

(12) Barlow, D. J.; Thornton, J. M. Helix Geometry in Proteins. *J. Mol. Biol.* **1988**, *201*, 601−619.

(13) Baker, E. N.; Hubbard, R. E. Hydrogen Bonding in Globular Proteins. *Prog. Biophys. Mol. Biol.* **1984**, *44*, 97−179.

(14) Thanki, N.; Thornton, J. M.; Goodfellow, J. M. Distributions of Water around Amino Acid Residues in Proteins. *J. Mol. Biol.* **1988**, *202*, 637−657.

(15) McColl, I. H.; Blanch, E. W.; Hecht, L.; Barron, L. D. A Study of a-Helix Hydration in Polypeptides, Proteins, and Viruses Using Vibrational Raman Optical Activity. *J. Am. Chem. Soc.* **2004**, *126*, 8181−8188.

(16) Barron, L. D.; Buckingham, A. D. Vibrational Optical Activity. *Chem. Phys. Lett.* **2010**, *492*, 199−213.

(17) Barron, L. D. *Molecular Light Scattering and Optical Activity*, 2nd ed.; Cambridge University Press: Cambridge, U.K., 2004.

(18) Nafie, L. A. *Vibrational Optical Activity: Principles and Applications*. John Wiley & Sons Ltd.: West Sussex, 2011.

(19) Hug, W. Measurement of Raman Optical Activity. In *Comprehensive Chiroptical Spectroscopy, Volume 1, Instrumentation, Methodologies, and Theoretical Simulations*, Berova, N.; Polavarapu, P. L.; Nakanishi, K.; Woody, R. W., Eds.; John Wiley & Sons, Ltd.: New Jersey, Canada, 2012; pp 147−178.

(20) Barron, L. D.; Buckingham, A. D. Rayleigh and Raman Scattering from Optically Active Molecules. *Mol. Phys.* **1971**, *20*, 1111−1119.

(21) Barron, L. D.; Bogaard, M. P.; Buckingham, A. D. Raman Scattering of Circularly Polarized Light by Optically Active Molecules. *J. Am. Chem. Soc.* **1973**, *95*, 603−605.

(22) Barron, L. D.; Hecht, L.; Blanch, E. W.; Bell, A. F. Solution Structure and Dynamics of Biomolecules from Raman Optical Activity. *Prog. Biophys. Mol. Biol.* **2000**, *73*, 1−49.

(23) Barron, L. D.; Hecht, L.; McColl, I. H.; Blanch, E. W. Raman Optical Activity Comes of Age. *Mol. Phys.* **2004**, *102*, 731−744.

(24) Barron, L. D.; Zhu, F.; Hecht, L. Raman Optical Activity: An Incisive Probe of Chirality, and of Biomolecular Structure and Behaviour. *Vib. Spectrosc.* **2006**, *42*, 15−24.

(25) Zhu, F.; Isaacs, N. W.; Hecht, L.; Barron, L. D. Raman Optical Activity: A Tool for Protein Structure Analysis. *Structure* **2005**, *13*, 1409−1419.

(26) Kinalwa, M.; Blanch, E. W.; Doig, A. J. Accurate Determination of Protein Secondary Structure Content from Raman and Raman Optical Activity Spectra. *Anal. Chem.* **2010**, *82*, 6347−6349.
(27) McColl, I. H.; Blanch, E. W.; Gill, A. C.; Rhie, A. G. O.; Ritchie, M. A.; Hecht, L.; Nielsen, K.; Barron, L. D. A New Perspective on B-Sheet Structures Using Vibrational Raman Optical Activity: From Poly(L-Lysine) to the Prion Protein. *J. Am. Chem. Soc.* **2003**, *125*, 10019−10026.
(28) Blanch, E. W.; Morozova-Roche, L. A.; Cochran, D. A. E.; Doig, A. J.; Hecht, L.; Barron, L. D. Is Polyproline Ii Helix the Killer Conformation? A Raman Optical Activity Study of the Amyloidogenic Prefibrillar Intermediate of Human Lysozyme. *J. Mol. Biol.* **2000**, *301*, 553−563.
(29) Blanch, E. W.; Morozova-Roche, L. A.; Hecht, L.; Noppe, W.; Barron, L. D. Raman Optical Activity Characterization of Native and Molten Globule States of Equine Lysozyme: Comparison with Hen Lysozyme and Bovine Alpha-Lactalbumin. *Biopolymers* **2000**, *57*, 235−248.
(30) Blanch, E. W.; Bell, A. F.; Hecht, L.; Day, L. A.; Barron, L. D. Raman Optical Activity of Filamentous Bacteriophages: Hydration of Alpha-Helices. *J. Mol. Biol.* **1999**, *290*, 1−7.
(31) Barron, L. D.; Blanch, E. W.; Hecht, L. Unfolded Proteins Studied by Raman Optical Activity. Unfolded Proteins. *Adv. Protein Chem.* **2002**, *62*, 51−90.
(32) McColl, I. H.; Blanch, E. W.; Hecht, L.; Kallenbach, N. R.; Barron, L. D. Vibrational Raman Optical Activity Characterization of Poly(L-Proline) II Helix in Alanine Oligopeptides. *J. Am. Chem. Soc.* **2004**, *126*, 5076−5077.
(33) Blanch, E. W.; Gill, A. C.; Rhie, A. G. O.; Hope, J.; Hecht, L.; Nielsen, K.; Barron, L. D. Raman Optical Activity Demonstrates Poly(L-Proline) II Helix in the N-Terminal Region of the Ovine Prion Protein: Implications for Function and Misfunction. *J. Mol. Biol.* **2004**, *343*, 467−476.
(34) Yamamoto, S.; Watarai, H. Raman Optical Activity Study on Insulin Amyloid- and Prefibril Intermediate. *Chirality* **2012**, *24*, 97−103.
(35) Lee, S. H.; Krimm, S. Polarized Raman Spectra of Oriented Films of a-Helical Poly(L-Alanine) and Its *N*-Deuterated Analogue. *J. Raman Spectrosc.* **1998**, *29*, 73−80.
(36) Lee, S. H.; Krimm, S. Ab Initio-Based Vibrational Analysis of a-Poly(L-Alanine). *Biopolymers* **1998**, *46*, 283−317.
(37) Goodman, M.; Toda, F.; Ueyama, N. Apparent Helix-Coil Transition for Poly(L-Alanine) as Measured by Nuclear Magnetic Resonance. *Proc. Natl. Acad. Sci. U.S.A.* **1973**, *70*, 331−333.
(38) Shoji, A.; Kawai, T.; Nishioka, A. Solution Properties of Poly(Alanine), 3^1h Nmr Study of Poly(Alanine)S in the Mixture of Chloroform and Trifluoroacetic Acid. *Makromol. Chem.* **1978**, *179*, 611−624.
(39) Parrish, J. R.; Blout, E. R. The Conformation of Poly-L-Alanine in Hexafluoroisopropanol. *Biopolymers* **1972**, *11*, 1001−1020.
(40) Schellman, J. A.; Schellman, C. In *The Proteins*, Neurath, H., Ed. Academic Press: New York, 1964; Vol. 2, p 1.
(41) Ruud, K.; Thorvaldsen, A. J. Theoretical Approaches to the Calculation of Raman Optical Activity Spectra. *Chirality* **2009**, *21*, E84−E67.
(42) Cheeseman, J. R.; Shaik, M. S.; Popelier, P. L. A.; Blanch, E. W. Calculation of Raman Optical Activity Spectra of Methyl-B-D-Glucose Incorporating a Full Molecular Dynamics Simulation of Hydration Effects. *J. Am. Chem. Soc.* **2011**, *133*, 4991−4997.
(43) Haesler, J.; Schindelholz, I.; Riguet, E.; Bochet, C. G.; Hug, W. Absolute Configuration of Chirally Deuterated Neopentane. *Nature* **2007**, *446*, 526−529.
(44) Buděšínský, M.; Daněček, P.; Bednárová, L.; Kapitán, J.; Baumruk, V.; Bouř, P. Comparison of Quantitative Conformer Analyses by Nuclear Magnetic Resonance and Raman Optical Activity Spectra for Model Dipeptides. *J. Phys. Chem. A* **2008**, *112*, 8633−8640.
(45) Kaminský, J.; Kapitán, J.; Baumruk, V.; Bednárová, L.; Bouř, P. Interpretation of Raman and Raman Optical Activity Spectra of a Flexible SugarDerivative, the Gluconic Acid Anion. *J. Phys. Chem. A* **2009**, *113*, 3594−3601.
(46) Hopmann, K. H.; Šebestík, J.; Novotná, J.; Stensen, W.; Urbanová, M.; Svenson, J.; Svendsen, J. S.; Bouř, P.; Ruud, K. Determining the Absolute Configuration of Two Marine Compounds Using Vibrational Chiroptical Spectroscopy. *J. Org. Chem.* **2012**, *77*, 858−869.
(47) Šebestík, J.; Bouř, P. Raman Optical Activity of Methyloxirane Gas and Liquid. *J. Phys. Chem. Lett.* **2011**, *2*, 498−502.
(48) Hopmann, K. H.; Ruud, K.; Pecul, M.; Dračínský, M.; Bouř, P. Explicit Versus Implicit Solvent Modeling of Raman Optical Activity Spectra. *J. Phys. Chem. B* **2011**, *115*, 4128−4137.
(49) Jacob, C. R.; Luber, S.; Reiher, M. Calculated Raman Optical Activity Signatures of Tryptophan Side Chains. *ChemPhysChem* **2008**, *9*, 2177−2188.
(50) Yamamoto, S.; Watarai, H.; Bouř, P. Monitoring the Backbone Conformation of Valinomycin by Raman Optical Activity. *ChemPhysChem* **2011**, *12*, 1509−1518.
(51) Yamamoto, S.; Straka, M.; Watarai, H.; Bouř, P. Formation and Structure of the Potassium Complex of Valinomycin in Solution Studied by Raman Optical Activity Spectroscopy. *Phys. Chem. Chem. Phys.* **2010**, *12*, 11021−11032.
(52) Profant, V.; Baumruk, V.; Li, X.; Šafařík, M.; Bouř, P. Tracking of the Polyproline Folding by Density Functional Computations and Raman Optical Activity Spectra. *J. Phys. Chem. B* **2011**, *115*, 15079−15089.
(53) Yamamoto, S.; Kaminský, J.; Bouř, P. Structure and Vibrational Motion of Insulin from Raman Optical Activity Spectra. *Anal. Chem.* **2012**, *84*, 2440−2451.
(54) Luber, S.; Reiher, M. Theoretical Raman Optical Activity Study of the B Domain of Rat Metallothionein. *J. Phys. Chem. B* **2010**, *114*, 1057−1063.
(55) Herrmann, C.; Ruud, K.; Reiher, M. Can Raman Optical Activity Separate Axial from Local Chirality? A Theoretical Study of Helical Deca-Alanine. *ChemPhysChem* **2006**, *7*, 2189−2196.
(56) Jacob, C. R.; Luber, S.; Reiher, M. Understanding the Signatures of Secondary-Structure Elements in Proteins with Raman Optical Activity Spectroscopy. *Chem.—Eur. J.* **2009**, *15*, 13491−13508.
(57) Luber, S. Solvent Effects in Calculated Vibrational Raman Optical Activity Spectra of *a*-Helices. *J. Phys. Chem. A* **2013**, *117*, 2760−2770.
(58) Bouř, P.; Keiderling, T. A. Partial Optimization of Molecular Geometry in Normal Coordinates and Use as a Tool for Simulation of Vibrational Spectra. *J. Chem. Phys.* **2002**, *117*, 4126−4132.
(59) Bouř, P. Convergence Properties of the Normal Mode Optimization and Its Combination with Molecular Geometry Constraints. *Collect. Czech. Chem. Commun.* **2005**, *70*, 1315−1340.
(60) Klamt, A. Cosmo and Cosmo-Rs. In *The Encyclopedia of Computational Chemistry*; Schleyer, P. R., Allinger, N. L., Clark, T., Gasteiger, J., Kollman, P. A., Schaefer, H. F., III; Schreiner, P. R., Eds. John Wiley & Sons: Chichester, U.K., 1998; Vol. *1*, pp 604−615.
(61) Cramer, C. J.; Truhlar, D. G. Implicit Solvation Models: Equilibria, Structure, Spectra and Dynamics. *Chem. Rev.* **1999**, *99*, 2161−2200.
(62) Bouř, P. On the Influence of the Water Electrostatic Field on the Amide Group Vibrational Frequencies. *J. Chem. Phys.* **2004**, *121*, 7545−7548.
(63) Hanwell, M. D.; Curtis, D. E.; Lnie, D. C.; Vandermeersch, T.; Zurek, E.; Hutchinson, G. R. Avogadro: An Advanced Semantic Chemical Editor, Visualization, and Analysis Platform. *J. Cheminformatics* **2012**, *4*, 17.
(64) Bouř, P.; Sopková, J.; Bednárová, L.; Maloň, P.; Keiderling, T. A. Transfer of Molecular Property Tensors in Cartesian Coordinates: A New Algorithm for Simulation of Vibrational Spectra. *J. Comput. Chem.* **1997**, *18*, 646−659.
(65) Yamamoto, S.; Li, X.; Ruud, K.; Bouř, P. Transferability of Various Molecular Property Tensors in Vibrational Spectroscopy. *J. Chem. Theory Comput.* **2012**, *8*, 977−985.

(66) Frisch, M. J.; Trucks, G. W.; Schlegel, H. B.; Scuseria, G. E.; Robb, M. A.; Cheeseman, J. R.; Scalmani, G.; Barone, V.; Mennucci, B.; Petersson, G. A., et al. *Gaussian 09*, Gaussian, Inc.: Wallingford CT, 2009.
(67) Becke, A. D. Density-Functional Thermochemistry. IV. A New Dynamical Correlation Functional and Implications for Exact-Exchange Mixing. *J. Chem. Phys.* **1993**, *98*, 5648−5652.
(68) Bouř, P.; Maloň, P. *Mcm Molecular Graphics*; Academy of Sciences: Prague, 2013.
(69) Bieler, N. S.; Haag, M. P.; Jacob, C. R.; Reiher, M. Analysis of the Cartesian Tensor Transfer Method for Calculating Vibrational Spectra of Polypeptides. *J. Chem. Theory Comput.* **2011**, *7*, 1867−1881.
(70) Rabolt, J. F.; Moore, W. H.; Krimm, S. Vibrational Analysis of Peptides, Polypeptides and Proteins. 3. α-Poly(L-Alanine). *Macromolecules* **1977**, *10*, 1065−1074.
(71) Kapitán, J.; Baumruk, V.; Kopecký, V., Jr.; Bouř, P. Conformational Flexibility of L-Alanine Zwitterion Determines Shapes of Raman and Raman Optical Activity Spectral Bands. *J. Phys. Chem. A* **2006**, *110*, 4689−4696.
(72) Kapitán, J.; Baumruk, V.; Kopecký, V., Jr.; Pohl, R.; Bouř, P. Proline Zwitterion Dynamics in Solution, Glass and Crystalline State. *J. Am. Chem. Soc.* **2006**, *128*, 13451−13462.
(73) Mukhopadhyay, P.; Zuber, G.; Beratan, D. N. Characterizing Aqueous Solution Conformations of a Peptide Backbone Using Raman Optical Activity Computations. *Biophys. J.* **2008**, *95*, 5574−5586.
(74) Grimme, S. Semiempirical Gga-Type Density Functional Constructed with a Long-Range Dispersion Correction. *J. Comput. Chem.* **2006**, *27*, 1787−1799.
(75) Perdew, J. P.; Burke, K.; Wang, Y. Generalized Gradient Approximation for the Exchange-Correlation Hole of a Many-Electron System. *Phys. Rev. B* **1996**, *54*, 16533−16539.
(76) Yanai, T.; Tew, D. P.; Handy, N. C. New Hybrid Exchange-Correlation Functional Using the Coulomb-Attenuating Method (Cam-B3lyp). *Chem. Phys. Lett.* **2004**, *393*, 51−57.
(77) Chai, J. D.; Head-Gordon, M. Long-Range Corrected Hybrid Density Functionals with Damped Atom-Atom Dispersion Corrections. *Phys. Chem. Chem. Phys.* **2008**, *10*, 6615−6620.
(78) Forge, V.; Wijesinha, R. T.; Balbach, J.; Brew, K.; Robinson, C. V.; Redfield, C.; Dobson, C. M. Rapid Collapse and Slow Structural Reorganisation During the Refolding of Bovine A-Lactalbumin. *J. Mol. Biol.* **1999**, *288*, 673−688.